Vera C. Rubin Observatory
Project Science Team

Updated estimates of the Rubin system throughput and expected LSST image depth

Federica B. Bianco, Lynne Jones, Željko Ivezić, Steven Ritz, and the Rubin Project Science Team

PSTN-054

Latest Revision: 2022-06-21

Abstract

This document presents updated estimates, as of May 2022, of the Rubin system throughput and compares them to throughput requirements from the LSST Science Requirements Document. In addition, it uses these estimates to forecast LSST's median single-visit and co-added image depths for the current (OpSim v2.0) baseline LSST cadence simulation: (23.8, 24.5, 24.0, 23.4, 22.7, 22.0) and (25.6, 26.9, 26.9, 26.4, 25.6, 24.8) in $ugrizy$, respectively. In addition, it uses these estimates to forecast LSST's median single-visit and co-added image depths for the current baseline LSST cadence simulation. Estimated system performance relies on actual measurements of the performance of various system hardware components, and on simulations where measurements are still unavailable. The updated performance estimates meet all the relevant requirements from the LSST Science Requirements Document. As our knowledge of the as-buit system continues to improve, updates to these estimates will continue to be provided.

Change Record

Version	Date	Description	Owner name
1	YYYY-MM-DD	Unreleased.	federica bianco (she/her/hers)

Document source location: `https://github.com/lsst-pst/pstn-054`

Contents

Updated estimates of the Rubin system throughput and expected LSST image depth

1   Introduction

The LSST System Science Requirements Document (LPM-17, hereafter SRD) lists the science-driven requirements for the data products to be delivered by LSST. Engineering requirements for each technical subsystem of the Rubin Observatory have been derived from this document.

The required overall system throughput is specified by requirements listed in the SRD Tables 5 and 6 (also reported in Table 1 of Ivezić et al. 2019). Those requirements primarily constrain the effective primary mirror diameter and overall (hardware + atmosphere) system throughput (*e.g.*, mirror surface reflectivity, sensor quantum efficiency). For ease of interpretation, Tables 5 and 6 express these requirements in terms of limiting image depth, m_5 (defined as a magnitude at which a photometric signal-to-noise ratio SNR=5 is attained), corresponding to **fiducial** observing parameters. These fiducial parameters include exposure time per visit (2×15 sec), delivered *r*-band seeing (0.7 arcsec), boresight airmass ($X = 1$) and *r*-band sky brightness (14.5 mJy arcsec^{-2}, equivalent to 21 AB mag arcsec^{-2}).

While these fiducial values were chosen to approximately correspond to realistic observing conditions, the m_5 values listed in Tables 5 and 6 should **not** be interpreted as expected LSST single-visit depths (for example, the telescope cannot even point towards the zenith such that $X > 1$ for all observations, and the fiducial sky brightness is approximately equivalent to astronomical *dark* sky brightness). In section 2 we derive the relevant quantities related to the SRD requirements with updated system and hardware component information. To predict the single-visit depth distribution and co-added image depth, cadence simulations that account for the variation of anticipated observing conditions are needed. These simulations are discussed in section 3. Finally, we discuss potential venues for optimization of the hardware elements and survey and the impact they would have on image depth in section 4.

2 Comparison of current throughput estimates with the SRD requirements

Given the measured or assumed performance of various system hardware components (including transmissivity and reflectivity for optical components, quantum efficiency for sensors, instrumental noise) and the fiducial observing parameters listed in the previous section, the corresponding limiting image depth is computed using a procedure described in LSE-40 and version-controlled code managed by Rubin Systems Engineering. The seeing is converted to the appropriate seeing per bandpass using a wavelength-dependent model described in Document-20160 and implemented in the `rubin_sim SeeingModel`. The sky brightness is converted to a per-band sky brightness using the dark sky spectral energy distribution (SED) documented in LSE-40.

Table 1 lists the minimum and design SRD requirements for m_5 (rows 1 and 2) and current best estimates for anticipated system performance for all six LSST bands ($ugrizy$, rows 3).We refer to the m_5 thus calculated as "m_5 SRD estimated". Estimation of these m_5 values assumes $X = 1$ and a total visit exposure time of 30 seconds, split between two 15-second exposures (2x15 sec "snaps"). The performance of each component in the hardware systems is based on the values kept up-to-date in the Rubin `syseng_throughputs` package, version 1.7. The reflectivity curves of the system optical surfaces are encoded in this package. It is assumed that the primary (*M1*), secondary (*M2*), and tertiary (*M3*) mirrors are coated with aluminium, silver, and aluminium respectively, and reflectivity estimates are based on measurements from coating samples from June 2019.

We derived the estimates of m_5 setting a readout noise equal to 8.8 e⁻/pixel/read-out. This corresponds to assuming readout noise equal to the system requirements readout noise across the entire CCD plane (see LSE-59). [1] This is a conservative choice, as the median readout noise is now measured to be well below system requirements (between 5 and 6 e⁻/pixel/read-out, see subsection 3.4). Measured, per-amplifier read-out noise values will be incorporated in the m_5 estimates in subsection 3.4.

---

[1]These requirements are for a maximum readout noise of 9 e⁻/pixel/read-out, but include an estimated 0.2 e⁻/pixel/read-out of dark currrent. Using 8.8 or 9 e⁻/pixel/read-out, however, generates negligible differences.

TABLE 1: Comparison of the SRD single visit magnitude sensitivity requirements and the system sensitivity estimates. The estimated seeing and sky brightness are also included (row 4 and 5).

row	m_5	u	g	r	i	z	y
1	m_5 SRD design	23.90	25.00	24.70	24.00	23.30	22.10
2	m_5 SRD minimum	23.40	24.60	24.30	23.60	22.90	21.70
3	m_5 SRD estimated	24.23	25.08	24.58	24.15	23.58	22.70
4	seeing (arcsec)	0.77	0.73	0.70	0.67	0.65	0.63
5	skybrightness (mag/arcsec^2)	22.72	22.07	21.00	20.27	19.39	18.43

The estimated m_5 values listed in the third row of Table 1 are fainter than the minimum SRD requirements (second row) in all six bands, with a substantial margin. In all bands except for the r band, estimated m_5 values are also fainter than the design SRD requirements listed in the first row.

In the r band, estimated m_5 is 0.12 mag brighter than the design SRD requirement. If desired, this difference in depth could be recovered by using a 25% longer exposure time in the r band, corresponding to increasing the nominal survey per-band observing allocation from 22.3% to 27.8% at the expense of other bands. Summed over all bands, these estimated m_5 values imply that the design SRD depths can be reached with only 73.7% of nominal observing time, implying a "throughput reserve" of 26.3%. The minimum SRD depths can be reached with only 34.8% of nominal observing time.

To reiterate, the current throughput estimates (and thus the m_5 estimated values) compare favorably with the SRD requirements on limiting magnitude, with estimated values exceeding the minimum requirements in all bands and overperforming the design requirements in all bands but r. However, the values of m_5 computed for these **fiducial** observing conditions, as codified in the SRD, should **not** be interpreted as typical image depths expected for the LSST data.

3   Current estimates of single-visit depth distribution and co-added image depth

As we progress towards the end of construction and start of operations, our knowledge of the properties of the as-built system is steadily improving leading to increasingly accurate

estimates of LSST's image depth.

Next, we describe a few methodological improvements for estimating image depth. In Table 2 we report again the SRD estimates of m_5 for the reader's convenience (the same values included in Table 1 row 3) together with all system contributions to m_5 (Δm's); these quantities are additive corrections to m_5, such that positive values are improvements (*i.e.* larger values imply deeper images).

In subsection 3.3 and subsection 3.5 we discuss the single-visit and co-added image depth distributions estimated for the current simulated baseline LSST cadence.

3.1   Methodological improvements for estimating image depth

Improved models for the delivered point-spread-function (PSF) lead to a significant improvement in the fidelity of PSF simulations compared to the Gaussian assumption upon which the SRD calculations relied. The final PSF is not expected to be a single- or double-Gaussian profile, but rather a PSF as derived from a von Karman phase power spectrum (Xin et al., 2018; Fétick et al., 2018). We provide a measurement of the equivalent, "effective" full width at half maximum seeing parameter (FWHM$_{\mathrm{Eff}}$) to facilitate calculation of the m_5 limiting magnitudes. Document-20160 describes how to combine the atmospheric component with the contributions from the telescope and dome to result in the delivered PSF and estimated FWHM$_{\mathrm{Eff}}$ (in the case of a single-Gaussian profile, FWHM and FWHM$_{\mathrm{Eff}}$ are identical by construction; for PSF profiles with more extended tails, such as the von Karman profile, FWHM$_{\mathrm{Eff}}$> FWHM). A combination of the change from a simple Gaussian FWHM to the von Karman profile, and slight increases in the expected contributions of the hardware system, result in an increase in the expected FWHM$_{\mathrm{Eff}}$, with a concurrent change in expected limiting magnitude. These changes are reported as "Δm PSF profile update" in Table 2.

In addition to an improved PSF model, the current seeing model is based on a more extensive baseline of recorded Differential Image Motion Monitor (DIMM) measurements from the Observatory's site (about 10 years) than was available at the time of writing the SRD (about 3 years). With this extended DIMM dataset, the expectation value for atmospheric contribution to the delivered image quality (FWHM$_{500}$ - the 500 nm wavelength atmospheric contribution to seeing at zenith) has increased from an estimated FWHM$_{500} = 0.60$ arcsec to FWHM$_{500} = 0.72$ arcsec. In other words, the first three years of DIMM data had better average seeing than the full 10-year dataset now available. RTN-022 describes the atmospheric

seeing data from which the model is built, and the distributions used in the simulations. The resulting impact on limiting magnitudes, "Δm median FWHM$_{500}$ update", is listed in Table 2 (row 3). This correction is the largest single entry in Table 2 in all bands except u.

An estimate of the average lifetime losses in throughput due to aging and system contamination can also be included in deriving m_5. While these losses are not strictly linear in time, but instead vary between maintenance intervals, the average expected losses over the 10-year survey are shown in Table 2 as "Δm system aging".

The visits in u band are currently projected to be collected as a single exposure of 30 sec, while all other bands use two 15-sec back-to-back exposures to obtain a combined visit time of 30 sec. This choice limits the impact of the read-out noise, which in u is not negligible compared to the background noise due to the faintness of the u band sky (Figure 1). This generates an improvement in u band depth shown in Table 2 as "Δm 1x30s u-band".

A small update in the expected dark sky background is applied, resulting in a small change in m_5. This update brings the sky background to the dark sky values used in the cadence simulations, where the sky brightness is modeled as in Yoachim et al. (2016) ("Δm dark sky update").

The values listed in Table 2 as "Δm combined" represent the correction to m_5 SRD estimated (Table 1) that, collectively, lead to a new m_5 estimate reported in Table 2 as "m_5 reference ($X = 1$, median FWHM$_{500}$, dark)".

TABLE 2: Impact of updated PSF and sky brightness models, system degradation, and changed assumptions on the exposure time on m_5. The m_5 SRD estimated quantities are reported in row 1 of this table (same as Table 1 row 3) for the reader's convenience.

		u	g	r	i	z	y
1	m_5 SRD estimated	24.23	25.08	24.58	24.15	23.58	22.70
2	Δm PSF profile update	-0.14	-0.13	-0.11	-0.11	-0.11	-0.12
3	Δm median FWHM$_{500}$ update	-0.19	-0.19	-0.18	-0.18	-0.18	-0.18
4	Δm system aging	-0.21	-0.14	-0.12	-0.12	-0.12	-0.11
5	Δm 1x30s u-band	0.18	0.00	0.00	0.00	0.00	0.00
6	Δm dark sky update	-0.01	0.02	0.05	0.05	0.02	0.09
7	Δm combined	-0.36	-0.44	-0.37	-0.36	-0.40	-0.33
8	m_5 reference ($X = 1$, median FWHM$_{500}$, dark)	23.87	24.64	24.21	23.79	23.18	22.37

3.2 Encoding the effects of observing conditions

The distribution of observing conditions can be estimated with the aid of cadence simulations. In the on-going process of optimizing the survey strategy (Bianco et al., 2021), Rubin Observatory produced hundreds of simulations of the 10-year survey with updated realistic expectations for the weather, seeing, and downtime distributions. The survey simulations implement a cadence strategy and derive the resulting pointings and image property for each visit (Naghib et al., 2019; Delgado & Reuter, 2016; Delgado et al., 2014). Given information about the system throughput, the image depth can be estimated for arbitrary observing conditions. The impact of observing conditions on limiting depth can be gauged from the following expression (see section 3.2 in the LSST Overview paper):

$$m_5 = C_m + 0.5\,(m_{\text{sky}} - 21) + 2.5\,\log_{10}\left(\frac{0.7\,\text{arcsec}}{\theta}\right) + 1.25\,\log_{10}\left(\frac{t_{\text{vis}}}{30\,\text{sec}}\right) - k_m\,(X - 1) + \Delta C_m(\tau), \quad (1)$$

where m_{sky} is the sky brightness (AB mag arcsec^{-2}), θ is seeing, t_{vis} is exposure time per visit, k_m is the atmospheric extinction coefficient, and X is the boresight airmass. The quantity C_m encodes all the system properties and does not depend on observing conditions. For the fiducial observing conditions discussed in section 2, $C_m = m_5$.[2] The impact of variations in sky brightness, exposure time per visit, or read-out noise (determined including the number of

---

[2]It is C_m that is constrained by the requirements listed in Tables 5 and 6 of the SRD.

exposures per visit) are encoded in the correction term $\Delta C_m(\tau)$:

$$\Delta C_m(\tau) = \Delta C_m^\infty - 1.25 \log_{10} \left[1 + \frac{10^{(0.8\,\Delta C_m^\infty)} - 1}{(\tau/\tau_{fiducial})} \right]. \tag{2}$$

Here ΔC_m^∞ is the loss of depth at the nominal value of t_{vis} and other parameters due to finite read-out noise. Its value is the largest in the u band (because of very dark sky and small sky noise, compared to read-out noise). The quantity τ is defined as

$$\tau = \frac{t_{\text{vis}}\, B_{\text{sky}}}{\sigma_r^2}, \tag{3}$$

where B_{sky} is the sky brightness in Jy arcsec^{-2} and σ_r is the read-out noise.

3.3   Single-visit depth distribution

The cadence simulations use a model to describe the expected sky brightness as a function of location on the sky, lunar phase, and time, as described in depth in Yoachim et al. (2016) and implemented in the Rubin maintained and version controlled `rubin_sim SkyBrightness` module. Similarly, the simulations can provide seasonally appropriate, expected per-band delivered seeing estimates.

The most recent set of simulations (referred to as `v2.0`) arises from the recommendations of the Survey Cadence Optimization Committee (SCOC[3]) which is charged with the responsibility to balanced community inputs and science priorities, examining the impact that observing choices have on the survey's scientific throughput, as assess by the scientific community itself. A science-driven survey optimization requires control over many survey parameters. These include constraints on image quality through seeing and sky brightness, which directly impact image depth, but also choices such as cadence and filter alternation that provide additional constraints on the sky location to be observed, which in turn affects the depth of an image. Hereafter we use the latest baseline cadence simulation v2.0 (`baseline_v2.0`) to derive the expected m_5 from C_m. Throughout this simulation, exposure time is assumed to be 30 seconds, split into two 15 seconds snaps for each filter except u. Contributions to the difference in the *simulated* per-visit m_5 compared to the reference m_5 (as derived in subsection 3.2 and reported in Table 2) are listed separately in Table 3 for airmass, sky brightness, and seeing, together with the median simulated m_5.

---

[3]The structure of the SCOC is described at https://www.lsst.org/content/charge-survey-cadence-optimization-committee-scoc. In the same page, the ongoing activities of the SCOC are documented.

The seeing, airmass, and sky brightness distribution associated with dropping the fiducial requirement of observing at $X = 1$ and including a distribution of observing conditions as generated by the survey simulations are shown in Figure 1 and also reported in Table 3, including their median and 25th/75th percentile values over the 10 years of the `baseline_v2.0` survey for each bandpass. Their combined contribution is reported as "Δm combined". Note that, as the simulated m_5 is measured directly as the median m_5 of the simulated observations, small inconsistencies between this value and the value calculated by adding the median Δm's reported in Table 3 to the reference m_5 are to be expected, in part due to the non-gaussian nature of the sky brightness distributions.

Our early estimates of the impact of sky brightness variation and seeing degradation due to non-zenith observations were based on assuming a median airmass of $X = 1.2$ and a sky brightness variation amplitude of ~0.4 mag. This resulted in a median sky brightness brighter by 0.2 mag compared to the fiducial values. The SRD estimate of the magnitude loss associated with observations away from $X = 1$ were, in fact, conservative ($\Delta m \sim -0.2$ to -0.3 mag, see the caption of Table 24 in SRD). However, additional corrections can now be included, such as the impact of observing in different lunar phases, leading to magnitude losses ranges $\Delta m \sim -0.2$ to -0.5 mag compared to observations conducted in idealized, fiducial conditions.
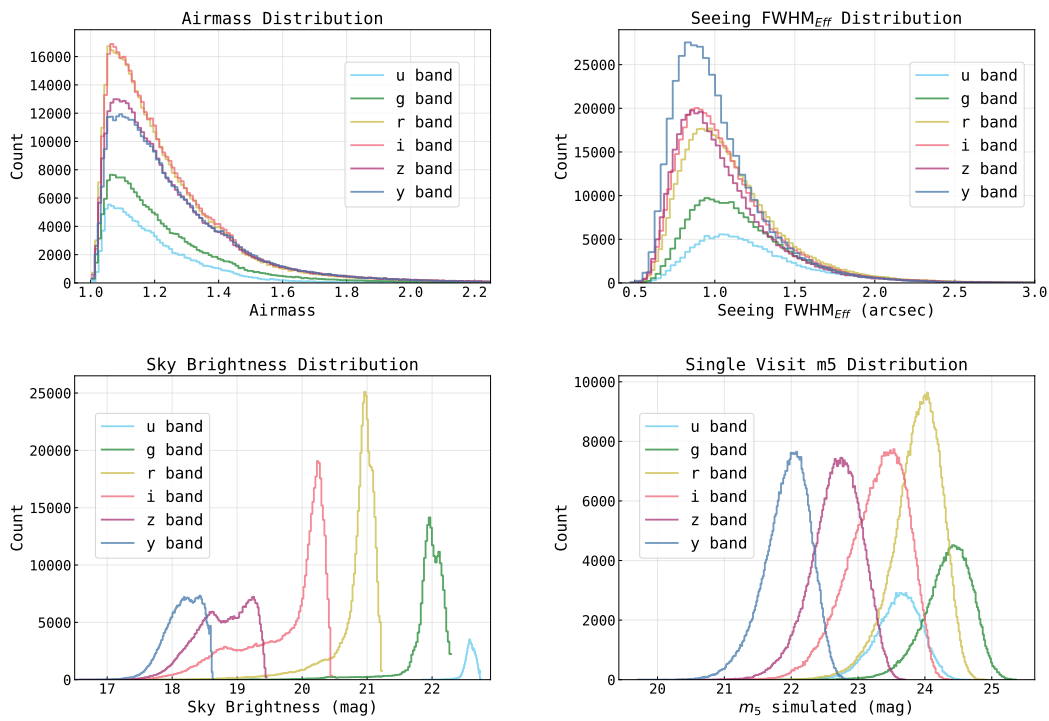
FIGURE 1: Distribution of airmass, seeing (FWHM$_{Eff}$, see subsection 3.1), sky brightness, and m_5 for the 10-year LSST survey simulated in `baseline_v2.0`, including Wide-Fast-Deep and minisurveys within.

TABLE 3: Simulated distributions of visit airmass, sky brightness, and seeing (FWHM$_{Eff}$, see subsection 3.1) and their impact on m_5 (Δm's). The m_5 reference is reported in row 1 in this table (same as Table 2 row 8) for the reader's convenience. The m_5 estimates resulting from survey simulations is reported for the `baseline_v2.0` LSST simulation. As these are calculated as medians over the 10-year simulation, small discrepancies between the reported m_5 simulated median values and those obtained correcting the m_5 reference values by the reported Δm combined are expected.

		u	g	r	i	z	y
m_5	reference	23.87	24.64	24.21	23.79	23.18	22.37
airmass	reference	1.00	1.00	1.00	1.00	1.00	1.00
	25th percentile	1.09	1.10	1.10	1.10	1.11	1.11
	median	1.16	1.18	1.18	1.18	1.19	1.20
	75th percentile	1.27	1.31	1.31	1.32	1.33	1.34
sky brightness	reference	22.68	22.11	21.11	20.39	19.43	18.63
	25th percentile	22.54	21.87	20.78	19.33	18.48	17.99
	median	22.59	21.98	20.94	20.01	18.80	18.20
	75th percentile	22.64	22.10	21.03	20.23	19.13	18.39
seeing FWHM$_{Eff}$	reference	1.04	0.98	0.92	0.88	0.86	0.84
	25th percentile	0.97	0.93	0.88	0.85	0.83	0.82
	median	1.16	1.11	1.05	1.01	0.97	0.95
	75th percentile	1.41	1.34	1.27	1.22	1.18	1.14
Δm airmass	25th percentile	-0.05	-0.02	-0.01	-0.01	-0.01	-0.02
	median	-0.08	-0.04	-0.02	-0.02	-0.01	-0.03
	75th percentile	-0.13	-0.07	-0.04	-0.03	-0.02	-0.06
Δm sky brightness	25th percentile	-0.07	-0.12	-0.17	-0.53	-0.48	-0.32
	median	-0.04	-0.07	-0.09	-0.19	-0.31	-0.22
	75th percentile	-0.02	-0.01	-0.04	-0.08	-0.15	-0.12
Δm seeing FWHM$_{Eff}$	25th percentile	0.08	0.05	0.05	0.04	0.03	0.03
	median	-0.12	-0.14	-0.14	-0.14	-0.14	-0.14
	75th percentile	-0.33	-0.35	-0.34	-0.35	-0.35	-0.34
Δm combined	median	-0.24	-0.25	-0.25	-0.35	-0.46	-0.39
m_5	simulated, median	23.62	24.38	23.92	23.34	22.70	21.97

3.4   Realistic per-amplifier characteristics and related corrections

In all of the work described above, the read-noise and Quantum Efficiency (QE) curve have been assumed to be constant across the entire focal plane. In reality, each CCD chip will have slightly different QE curves and each amplifier will have a different read-noise value. Notably, Rubin's camera uses CCD chips produced by two different vendors, which have different characteristic QE and read-noise values. As mentioned earlier, assuming 8.8 e⁻/pixel/read-out as the single read-noise value is a conservative choice as the median noise per amp is significantly lower (Figure 2). The QE values used in the presented calculations assume a "joint" vendor QE curve, which is defined as the minimum QE value at each wavelength; as such, it does not truly represent the expected performance as a function of wavelength for either vendor, but rather the likely most conservative estimate. Vignetting effects also impact the limiting magnitudes near the edges of the field of view, and this effect has not been taken into account in the calculations presented thus far. For the filter throughput curves, the filter requirements, encoded in the `syseng_throughputs`, are adopted.

As CCDs have been delivered to the project, measurements of the expected read-noise, QE curves, and vignetting have been carried out for each amplifier. While incorporating these per-amp measurements in the 10-year survey simulations would be computationally impractical, slowing down the simulations significantly, their effect can be encoded through Equation 1 and Equation 2 applied to the m_5 reference from which the simulations are derived, assuming median values. Applying Δm combined (as shown in Table 3) as an additive factor to the "m_5 reference, corrected" values reported in Table 4 would lead to a new, "m_5 simulated corrected", representing the final expected single-image depths based on `baseline_v2.0` (reported in Table 4).

The distribution of read-noise for all camera amplifiers is shown in Figure 2 and the correction associated with read-noise, QE, as well as vignetting effects is shown in terms of ΔC_m in Figure 3 for each amplifier in the CCD plane in the u and y bands (where the effects are most and least significant, respectively). The per filter corrections applied to m_5 reference via Equation 1 and Equation 2 (including the QE and vignetting in ΔC_m^∞), are also reported in Table 4, as well as how they propagate to m_5 simulated.

TABLE 4: Corrections associated with per-amp read-noise, QE, and vignetting, their mean values and Inter-Quartile Range (IQR) across the CCD plame, and their impact on m_5 reference and m_5 simulated.

|		u	g	r	i	z	y
m_5	reference	23.87	24.64	24.21	23.79	23.18	22.37
C_m	reference	23.46	24.45	24.45	24.35	24.19	23.75
	per amp median	23.64	24.58	24.56	24.42	24.23	23.75
	per amp IQR	0.15	0.08	0.08	0.04	0.03	0.06
ΔC_m^∞	reference	0.28	0.15	0.09	0.06	0.04	0.03
	per amp median	0.15	0.07	0.04	0.03	0.02	0.02
	per amp IQR	0.07	0.03	0.02	0.01	0.01	0.00
m_5	reference, corrected	24.05	24.77	24.32	23.86	23.22	22.37
	simulated median, corrected	23.80	24.50	24.03	23.41	22.74	21.96
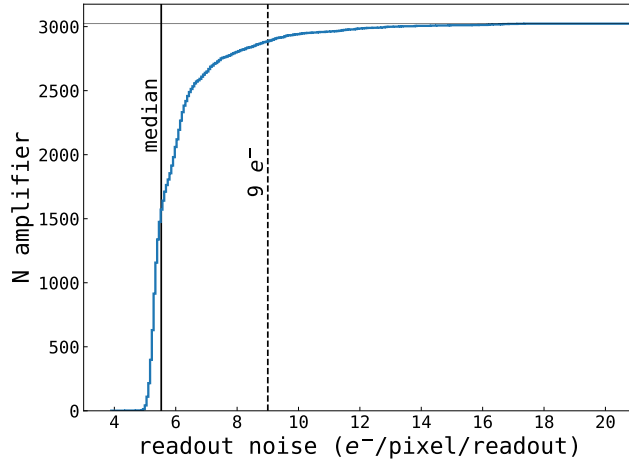
FIGURE 2: Readout noise cumulative distribution for the 3024 CCD segments (aka amplifiers) on the focal plane of the Camera. The values are from Camera test run 13283, using bias images taken using Version 26 of the sequencer, with the full camera in operation and analyzed with the Camera EOTest package. This run was also used for Camera Requirement Verification. The median noise is measured to be $\sim$5.5 e^-/pixel/readout, well below the requirement of 9 e^-/pixel/readout. The distribution shows a tail with 95% of the amplifiers within 9 e^-/pixel/readout. Vertical lines mark the median and nominal 9 e^-/pixel/readout noise values. One bad segment is not shown in the distribution.

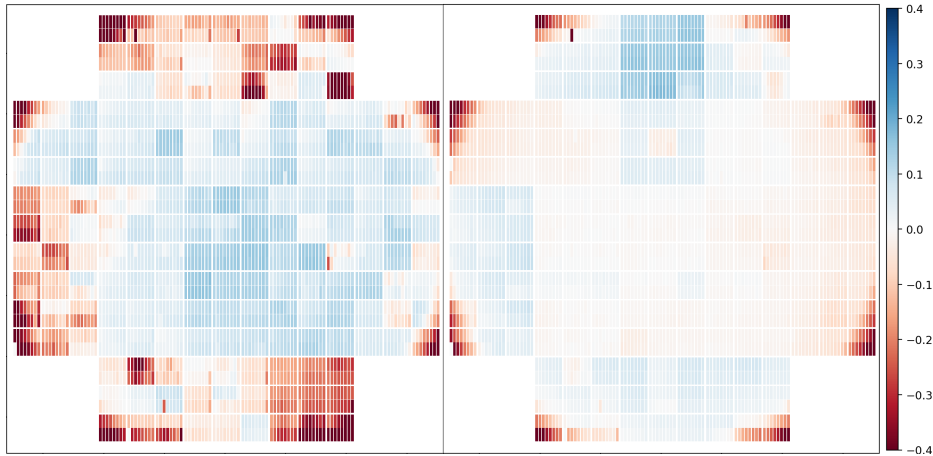FIGURE 3: The u (left) and y band (right) ΔCm corrections associated with read-noise, QE, and vignetting effects for each amplifier in the LSST DOE Camera CCD plane. The u and y bands represent the most extreme and most modest correction and correction IQR values, respectively (see Table 4).

3.5 Co-added depth distribution

With the survey simulations in hand, we can calculate the expected coadded depth in each band. The final coadded depth is dependent on the number of visits acquired at any point in

the sky, as well as on the individual image depths. These quantities are strongly dependent on survey strategy, although they are flexible within the limitations set by the total survey lifetime, minimum survey area, and observing duty-cycle requirements. Table 24 of the SRD reports an illustrative example of the LSST number of visits per bandpass and the corresponding idealised coadded depth of the survey, consistent with the assumption of a single image m_5 values as reported in Table 6 of SRD (and included in Table 1, row 1, of this document). We can now update these values with current survey simulations and using a realistic disstribution of m_5 values calculated as described above.

There is a trade-off between the total number of visits per field and the area covered to a specified depth. The SRD specifies minimum and design values for both the area covered and the median number of visits per pointing over that area in Tables 22 and 23: minimum values corresponding to a median of 750 visits per pointing over 15,000 sq. degrees, and design values of 825 visits per pointing over 18,000 sq. degrees. This footprint and the corresponding survey are referred to as the "Wide Fast Deep", hereafter WFD. In `baseline_v2.0`, 18,620 sq. degrees of sky receive at least 750 observations, with a median value of 829 visits per pointing over the same area. Conversely, an 18,000 square degree area receives a median of 839 visits. This represents an increase in footprint and number of visits over the illustrative values stated in the SRD. The per-band median number of visits per pointing over the 18,620 sq. degree WFD footprint are listed in Table 5, together with the resulting coadded depths calculated using the pointing histories simulated in `baseline_v2.0`.

As part of the SCOC work to define the survey footprint used for `baseline_v2.0`, trades between total area covered and number of visits per pointing were considered (see PSTN-053). The current footprint represents the result of this optimization and meets and exceeds the design requirements. These depths are consistent with the median individual image depths from Table 2, scaled by the median number of visits per pointing, reinforcing that most visits are obtained in or near median conditions.

TABLE 5: WFD visits per pointing and coadded depths. The 10-year LSST depth is reported as the median across all fields in the survey footprint in `baseline_v2.0` before and after correcting for the read-noise, QE, and vignetting effects as they vary across the CCD plane (see Table 4 and subsection 3.4)

		u	g	r	i	z	y
number of visits	25th percentile	53.0	70.0	178.0	181.0	160.0	164.0
	median	56.0	74.0	184.0	187.0	166.0	171.0
	75th percentile	59.0	78.0	190.0	193.0	173.0	178.0
m_5 median coadded		25.4	26.8	26.8	26.3	25.6	24.8
m_5 median coadded corrected		25.6	26.9	26.9	26.4	25.6	24.8

4 Further optimization options

The m_5 estimates reported in Table 3 can be further optimized, if desired, to increase the per visit or coadded depth of the survey.

As discussed in section 2, exposure time could be reassigned between bands. This would increase the m_5 in some bands, at the cost of a decrease in others.

A substantive fraction of the visits in `baseline_v2.0` were, in fact, collected as part of mini-surveys (see LSST Overview paper), and these observations could be redirected, if desired, to cover the WFD footprint in the main LSST survey, thus increasing the coadded m_5. In the `baseline_v2.0`, the fraction of images collected as part of surveys other than the WFD corresponds to about $\sim 34\%$. This implies that, in principle, the `baseline_v2.0` WFD has a "reserve" corresponding to ~ 280 images per field. The decision of reassigning these images to the WFD requires analyzing and balancing science priorities, and the SCOC is charged with performing this balancing exercise. Similarly, the distribution of visits between filters is under consideration by the SCOC. The distribution shown in Table 5 reflects current SCOC guidance, and also generally matches the illustrative distribution provided in Table 24 of the SRD.

The derived estimates of m_5 presented in Table 2 assume two exposures per visit to a combined $t_{vis} = 30$ seconds, except in u band. Abolishing the two-snap strategy would provide an improvement in efficiency via a decrease in overtime by about 8%. This time could be used to increase the observed footprint, the number of visits for pointing, or the total exposure in all or some bands. Each one of these choices, however, should also be vetted against the resulting image quality, image processing requirements, and overall scientific throughput of the survey.

Finally, the reported expected m_5 values assume current estimates of the mirrors' reflectivities, as discussed in section 2, which are still being optimized, filter coating transmission functions which will soon be updated with as-built measurements, as well as a surveying efficiency that remains to be demonstrated after the observatory is completed and enters its operations phase.

A   References

Bianco, F.B., Ivezić, Ž., Jones, R.L., et al., 2021, The Astrophysical Journal Supplement Series, 258, 1, URL `https://doi.org/10.3847/1538-4365/ac3e72`, doi:10.3847/1538-4365/ac3e72

Delgado, F., Reuter, M.A., 2016, In: Observatory Operations: Strategies, Processes, and Systems VI, vol. 9910 of Proc. SPIE, 991013, doi:10.1117/12.2233630, ADS Link

Delgado, F., Saha, A., Chandrasekharan, S., et al., 2014, In: Angeli, G.Z., Dierickx, P. (eds.) Modeling, Systems Engineering, and Project Management for Astronomy VI, vol. 9150 of Society of Photo-Optical Instrumentation Engineers (SPIE) Conference Series, 15, doi:10.1117/12.2056898, ADS Link

Fétick, R., Neichel, B., Mugnier, L.M., Montmerle-Bonnefois, A., Fusco, T., 2018, arXiv preprint arXiv:1809.06785

Ivezić, Ž., Kahn, S.M., Tyson, J.A., et al., 2019, ApJ, 873, 111 (`arXiv:0805.2366`), doi:10.3847/1538-4357/ab042c, ADS Link

Naghib, E., Yoachim, P., Vanderbei, R.J., Connolly, A.J., Jones, R.L., 2019, AJ, 157, 151 (`arXiv:1810.04815`), doi:10.3847/1538-3881/aafece, ADS Link

Xin, B., Ivezić, Ž., Lupton, R.H., et al., 2018, The Astronomical Journal, 156, 222, URL `https://doi.org/10.3847/1538-3881/aae316`, doi:10.3847/1538-3881/aae316

Yoachim, P., Coughlin, M., Angeli, G.Z., et al., 2016, Observatory Operations: Strategies, Processes, and Systems VI, URL `https://www.osti.gov/biblio/1784946`, doi:10.1117/12.2232947

B   Acronyms

Acronym	Description
B	Byte (8 bit)
CCD	Charge-Coupled Device
DIMM	Differential Image Motion Monitor
DOE	Department of Energy
FWHM	Full Width at Half-Maximum
LPM	LSST Project Management (Document Handle)
LSE	LSST Systems Engineering (Document Handle)
LSST	Legacy Survey of Space and Time (formerly Large Synoptic Survey Telescope)
M1	primary mirror
M2	Secondary Mirror
M3	tertiary mirror
OpSim	Operations Simulation
PSF	Point Spread Function
PST	Project Science Team
PSTN	Project Science Technical Note
QE	quantum efficiency
RTN	Rubin Technical Note
SCOC	Survey Cadence Optimization Committee
SED	Spectral Energy Distribution
SNR	Signal to Noise Ratio
SRD	LSST Science Requirements; LPM-17
WFD	Wide Fast Deep
arcsec	arcsecond second of arc (unit of angle)